Nanoscale Advances

ROYAL SOCIETY OF CHEMISTRY

PAPER

Cite this: *Nanoscale Adv.*, 2024, **6**, 3146

Insights into emulsion synthesis of self-assembled suprastructures formed by Janus silica particles with $-NH_2/-SH$ surface groups†

Inna V. Melnyk, *[ab] Veronika Tomina,[a] Halyna Yankovych,[b] Hristo Kolev, [c] Erika Dutkova, [b] Troy C. Breijaert,[d] Vadim G. Kessler[d] and Gulaim A. Seisenbaeva *[d]

Spherical particles with tunable anisotropic structures enabled by multiple surface functionalities have garnered interest for their potential applications in adsorption technologies. The presence of diverse functional groups in the surface layer, exhibiting varying acidity and hydrophilicity, can lead to unique characteristics in terms of surface structure and behaviour. In this study, the particles were synthesised using a two-step approach involving surface functionalisation of previously synthesised SiO_2 Stöber particles. This was achieved by employing 3-mercaptopropyltrimethoxysilane (MPTMS) and 3-aminopropyltrimethoxysilane (APTMS) in a toluene-in-water emulsion. The resulting particles were found to be nonporous, with a specific surface area of 8 m^2 g^{-1}. Their sizes were determined to be up to 350 nm through photon cross-correlation spectroscopy. Moreover, the particles exhibited a high net content of functional groups (both amino and mercapto) of 2 mmol g^{-1}. The organisation of the particles during synthesis was observed through SEM images, providing insights into their structural characteristics. Additionally, the study of Eu(III), Au(III), and Ag(I) ions and fluorescein adsorption demonstrated varying interactions on the surface, highlighting the potential applications and versatility of these functionalised particles.

Received 20th October 2023
Accepted 24th April 2024

DOI: 10.1039/d3na00909b

rsc.li/nanoscale-advances

Introduction

The principle of unity and conflict of opposites represents a fundamental law of dialectics, which underpins the self-propelling motion and evolution of natural phenomena. 'Janus particles' is a term broadly applied to colloids, nanoparticles, and other entities characterised by the distinct properties of their constituent parts. Typically, these entities are composed of two halves, each exhibiting unique characteristics. Presently, Janus particles find extensive applications across a myriad of human endeavours. These applications range from anti-cancer therapy in the medical field to the fabrication of solar cells and the development of ultra-thin, flexible video displays.

Janus particles have gained significant attention in the field of materials science due to their unique properties and versatile applications. The asymmetric structure allows Janus particles to exhibit interesting behaviours and functions that are not achievable with conventional particles.

The concept of Janus particles was introduced by Walther and Müller,[1] and numerous studies have been conducted to explore their synthesis, characterisation, and applications. Janus particles can be fabricated using various methods such as emulsion polymerisation, microfluidics, and template-assisted self-assembly.[2] These techniques enable precise control over the size, shape, composition, and surface functionality of Janus particles, leading to tailored properties for specific applications.

The unique feature of Janus particles lies in their asymmetric surfaces, which can have different chemical functionalities, charge distributions, or wettabilities. This enables Janus particles to exhibit a wide range of properties such as enhanced colloidal stability, selective adsorption, controlled self-assembly, and unique catalytic behaviour.[3] For example, Janus particles can be used as effective surfactants, stabilising emulsions and foams due to their amphiphilic nature.[4] They have also been utilised in drug delivery systems, where one side of the particle can encapsulate the drug, while the other side facilitates targeting or controlled release.[5]

[a]*Chuiko Institute of Surface Chemistry of NAS of Ukraine, 17, Generala Naumova Str., Kyiv 03164, Ukraine. E-mail: in.melnyk@gmail.com*

[b]*Institute of Geotechnics, Slovak Academy of Sciences, 45, Watsonova Str., Kosice 04001, Slovak Republic*

[c]*Institute of Catalysis, Bulgarian Academy of Sciences, 11, Acad. G. Bonchev Str., Sofia 1113, Bulgaria*

[d]*Department of Molecular Sciences, Swedish University of Agricultural Sciences, Box 7015, 5, Almas allé, Uppsala 75007, Sweden. E-mail: gulaim.seisenbaeva@slu.se*

† Electronic supplementary information (ESI) available. See DOI: https://doi.org/10.1039/d3na00909b

Moreover, Janus particles have shown promise in the field of optics and photonics. By incorporating different materials on each side, they can exhibit interesting optical properties such as plasmonic resonances, photonic bandgaps, and nonlinear optical responses.[6] This opens up possibilities for applications in sensing, imaging, and optical devices.

Since the declaration of 17 Sustainable Development Goals established by the United Nations in 2015,[7] the development of synthetic biocompatible materials with amphiphilic properties to decontaminate water and to promote well-being for all have been priority tasks to ensure healthy lives. Janus particles are sustainable materials with assembled architecture and significant environmentally friendly potential that have not been fully explored yet.[8] As a proof of concept, the interest in these materials has grown significantly over the past 10 years, as evidenced by their pilot applications for monitoring water and food quality,[9] bacteria imagining and toxin sensing,[10] metal identification,[11] the removal of microplastics,[12] water splitting,[13] and other uses.[14] Moreover, due to their anisotropic properties and tunable functionality, Janus nanoparticles can be utilised in bioimaging, biosensing, and drug delivery systems.[15]

The existence of amino and thiol groups is a kind of conflict of opposites. Amino and thiol groups are both functional groups that play important roles in various chemical reactions and biological processes. Thiol groups are highly reactive and can participate in redox reactions. They are important in protein structure and function, and are involved in various biological processes, including enzymatic reactions, detoxification, and cellular signalling. Both amino and thiol groups are crucial in the field of biochemistry and are extensively used in research and practical applications. Amino groups are often targeted for chemical modifications in drug development to enhance drug stability, solubility, and target specificity. Thiol groups are used in the synthesis of small molecules and bioconjugates, as well as in the preparation of gold nanoparticles and other nanomaterials. Therefore, grafting a silica surface with both types of groups at the same time is interesting and was previously studied by us[16–18] and other researchers.[19–21]

In this study, we tried to obtain Janus particles by emulsion synthesis, where thiol groups should get deposited in a hydrophobic solvent, and amino groups should be grafted in the hydrophilic solvent. In addition, particles, self-assemble to form spherical suprastructures. Their asymmetric structure allows for tailoring functionalities and opens up new opportunities in various fields. Adsorption of silver(I), gold(III), and europium(III) ions as well as fluorescein on the obtained particles was studied. These three ions and fluorescein were chosen for specific reasons. Firstly, both our research and the work of other scientists have demonstrated that mercapto groups have an affinity for gold and silver, while amino groups show an affinity for REEs and dyes. Secondly, from a practical standpoint, this choice holds significance in the field of environmental chemistry and biomedicine. This is because it enables a particle to carry both a luminescent marker and an antibacterial or anticancer marker concurrently.

The novelty and originality of the one-step grafting *via* Pickering emulsion[22] synthesis of self-assembled suprastructures formed by Janus silica particles with $-NH_2$ (amine) and –SH (thiol) surface groups are indeed significant in the field of materials science. This research intersects several advanced fields: nanotechnology, surface chemistry, and self-assembly processes.

The combination of these elements (duality, self-assembly, distinct reactivity and interaction patterns, and well-defined architecture) into a single study opens up new possibilities in the design of advanced materials.

Results and discussion

The creation of Janus particles involved a two-step process, as illustrated in Fig. 1. Initially, silica particles, each approximately 250 nm in size, were synthesised (refer to Fig. 2a and b). During the synthesis, TEOS-based sol was subjected to a heating process aimed at reducing particle size, based on the observation that heating silica precursor TEOS alone leads to smaller particle sizes.[23] Subsequent to this size reduction, the silica particles underwent a functionalisation process within a Pickering emulsion. This step involved the introduction of hydrolysed silanes into the emulsion. Specifically, a silane compound with a thiol group was mixed beforehand with toluene. The pre-hydrolysis process for aminosilane was facilitated using a water solution of fluoride ions, while for mercaptosilane, hydrochloric acid was used. It was hypothesised (relying on the solubility of the silanes) that, upon immersion in the emulsion, the silica particles would distribute evenly at the border between the water and toluene phases, aligning the amino groups in water and the mercapto groups in toluene. The successful execution of this process, as depicted in Fig. 1, led to the formation of the desired Janus particles.

It should also be noted that the functionalisation of silica particles using the proposed method with only one silane does not lead to the formation of the macrostructures and a stable coating on silica spheres. It is possible to assume that an emulsion involves components with differing hydrophobic (water-repelling) and hydrophilic (water-attracting) properties.

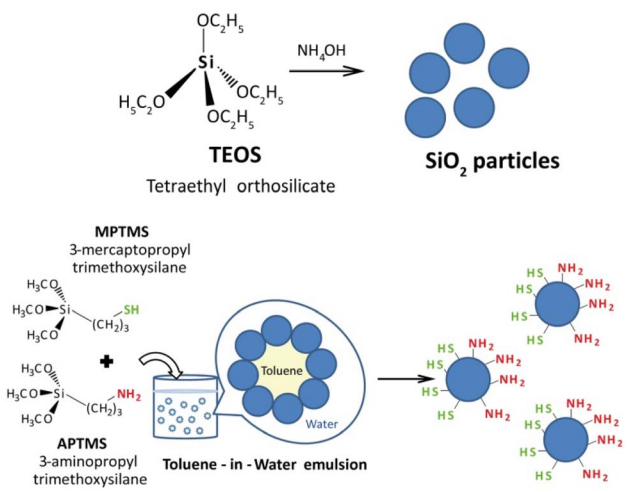

Fig. 1 Scheme of the synthesis and functionalisation of SiO_2 particles.

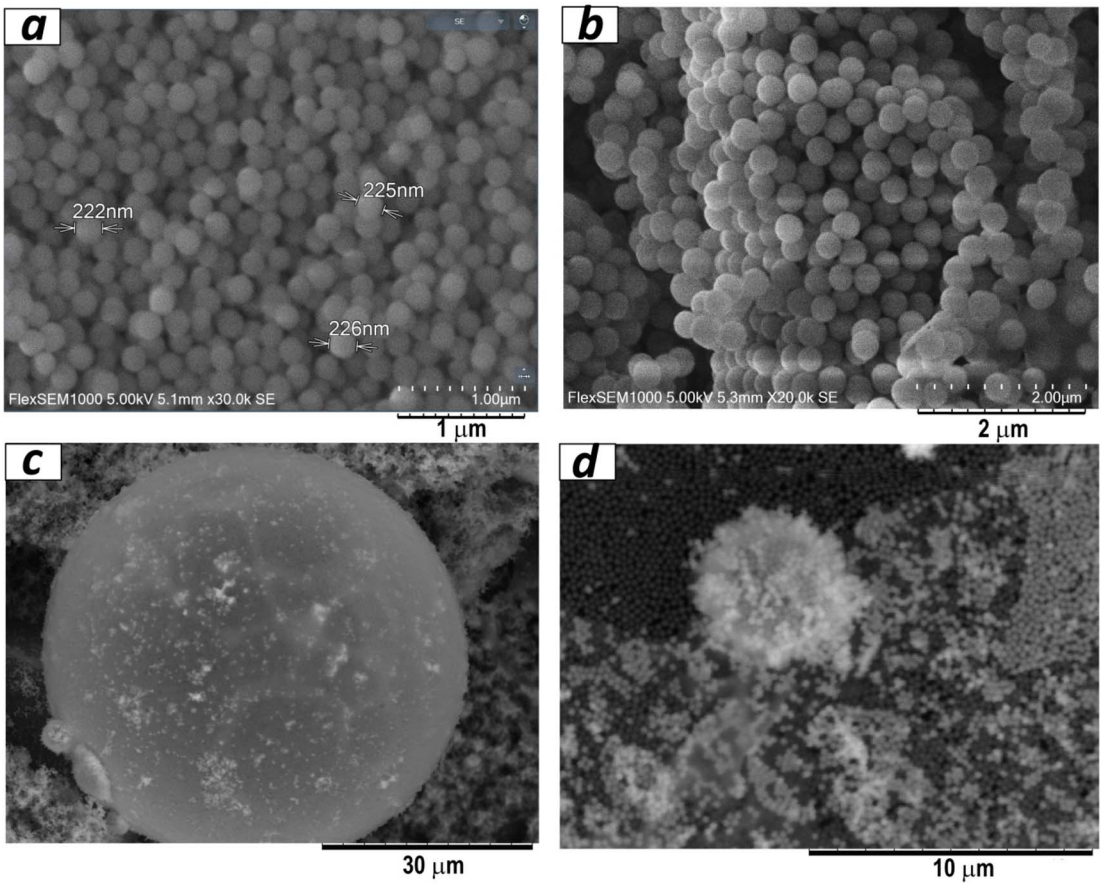

Fig. 2 SEM images of initial SiO_2 particles (a and b) and SiO_2/–SH/–NH_2 particles (c and d).

These differences lead to the segregation of components at interfaces, promoting self-assembly to achieve a more stable configuration.

Suprastructures formed through self-assembly can contribute to the stability of emulsions.[24] For instance, amphiphilic molecules (containing both hydrophobic and hydrophilic parts) tend to align at interfaces, creating a protective layer that prevents coalescence of droplets. As well, charged components in emulsions can interact through electrostatic forces, leading to the formation of ordered structures. Electrostatic attraction or repulsion between particles can influence their arrangement and stability. Thus, by using only one component (silane) in this system, we lose a set of opposite features that ensure the formation of superstructures.

The bifunctional particles thus produced self-organised into ball-shaped structures of different sizes, from 5 to 30 μm (Fig. 2c and d). Such a kind of structure opens up additional possibilities for applications. Additionally, AFM data (Fig. 3) indicated that the silica particles consisted of primary particles ranging in size from 5 to 10 nm, while the observed SEM images showed the formation of 250 nm spherical particles as agglomerates of these primary particles. Consequently, the synthesis process involves the formation of spherical silica particles with sizes up to 10 nm, which further assemble into 250 nm particles, and eventually organise into suprastructures within emulsions reaching sizes up to 30 μm.[25]

In order to investigate the obtained Janus particles, SEM-EDXS mapping was performed for two elements (Fig. 4). The mapping results, as depicted in Fig. 4, reveal that even at a macrostructural level, the particles exhibit an arrangement where different parts are exposed outward, alternating between amino and mercapto groups, creating a kind of "cranberry" pattern. It is challenging to determine from this method whether a particle is entirely covered with amino groups or mercapto groups. Evidently, the functionalization occurs in patches, indicating that these Janus particles can be categorised as Janus patches.[26]

The shapes of nitrogen adsorption–desorption isotherms of pristine SiO_2 and bifunctional silica particles allows us to assign these materials to non-porous materials with Type II isotherms.[27] The incorporation of amino- and sulphur-containing functional groups caused a significant reduction of the S_{BET} of SiO_2/–SH/–NH_2 in comparison to the original silica, which can be explained by particle agglomeration during synthesis. The total pore volume decreased from $V_{tot} = 0.153$ $cm^3\ g^{-1}$ to 0.044 $cm^3\ g^{-1}$, although the pore size has increased (Fig. S1†). According to particle size distribution (Fig. 5a), it can be seen that bifunctional silica particles possessed a larger size – 352 nm, whereas bare silica led to particles with a size of 269 nm. This can be explained by the particles' agglomeration caused by their charge and structural features (AFM and SEM data). An interesting observation has been made based on zeta-

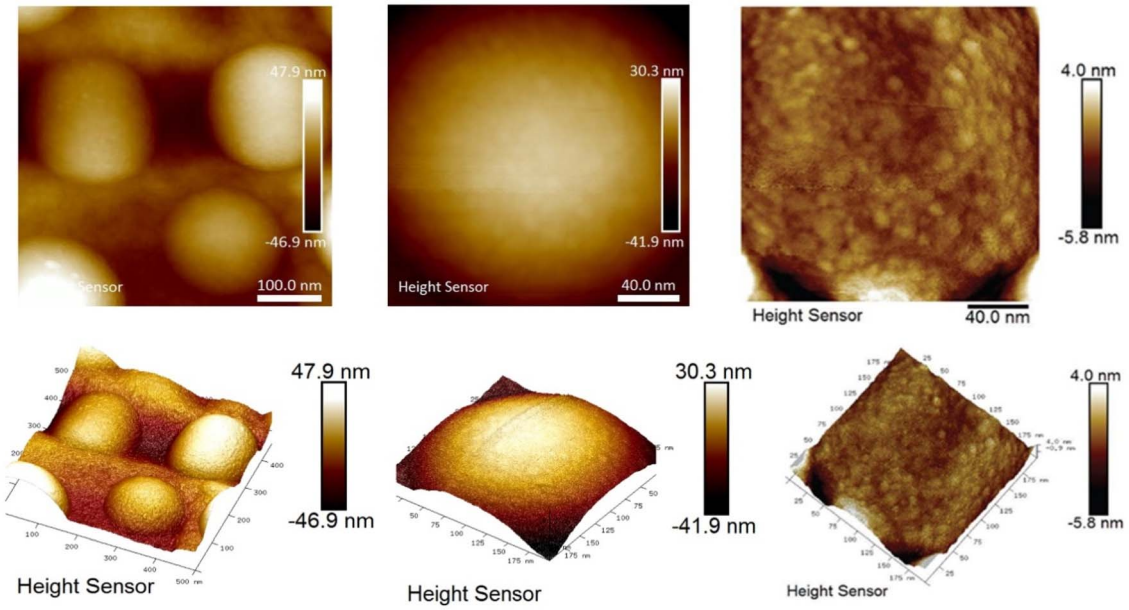

Fig. 3 AFM images of SiO_2/–SH/–NH_2 particles at different magnifications.

potential measurements, proving a more basic nature of modified silica particles: the point of zero charge for pristine SiO_2 was 3.0 and for SiO_2/–SH/–NH_2 was 5.8 (Fig. 5b). This fact can be interpreted by the presence of acidic –SH and basic –NH_2 surface groups. Although we have shown for bifunctional xerogels that no zwitterion is formed,[16] the surface contains acidic and basic groups and, as a result, both groups contribute to the pH of the equivalence point.

The number of amino and thiol groups was determined by various methods (Table 1): in elemental analysis, it was determined by the total amounts of nitrogen and sulphur; in titration and interaction with Ellman's reagent, by the number of groups available for interaction in the solution. The amount of N and S on the surface was also determined by the EDXS and XPS methods. Each method employed in the study has its own limitations and drawbacks; however, the results obtained from different methods correlated with each other overall. Based on this correlation, it could be concluded that, when using this synthesis method, the surface of the silica particles contained approximately 2 mmol g^{-1} of both amino and mercapto groups. Additionally, TGA data (Fig. S2†) provided further confirmation for the presence of groups on the surface of the silica particles. The organic component showed a weight loss of approximately 24%, which corresponded well to ~2 mmol g^{-1} in terms of the number of groups.

Fig. 6 displays the FTIR spectra of the materials. In all samples, a notable absorption in the 1000–1200 cm^{-1} region was observed, which was attributed to the presence of a three-dimensional siloxane bond within the material's skeletal structure. The presence of –CH_2–, –CH_3 groups was evident from a group of weak intensity bands observed in the 1300–1500 cm^{-1} region, as well as two bands in the 2800–3000 cm^{-1} region.[28] These latter bands were attributed to valence vibrations ($\nu_{s,as}$) of the CH bonds. It should be noted that pure silica also contained these bands, which indicated the existence of residual ethoxy groups on its surface and incomplete hydrolysis. The presence of thiol groups in the IR spectra of the SiO_2/–SH/–NH_2 sample (shown in Fig. 6, two lower spectra), was indicated by a low-intensity absorption band at 2563 cm^{-1}, which was assigned to the stretching vibration (ν) of the –SH group.[29] The spectra of the functionalised samples exhibited bending vibrations of amino groups, which were observed at 1591 cm^{-1}. The occurrence of water in all samples was evident from the vibrations observed in the 1600–1650 cm^{-1} range, attributed to the $\delta(H_2O)$ vibrations, and the broad band around 3300 cm^{-1} corresponding to the ν(OH) vibrations of the adsorbed water. However, upon heating the sample, the physically adsorbed water was partially eliminated, leading to the emergence of distinct bands corresponding to the stretching vibrations of N–H in the amino groups, which became clearly visible at 3357 and 3292 cm^{-1}. As well, all samples displayed a band at 3640 cm^{-1} that belongs to silanol groups, and its intensity decreased in the functionalised SiO_2/–SH/–NH_2 sample. Thus, IR spectroscopy confirmed the functionalisation of silica particles with 3-aminopropyl and 3-mercaptopropyl silanes.

The patchy nature of the surface of obtained adsorbents could be clearly traced applying Quantitative Peak Force Management (QPFM) approach in AFM (see Fig. 7 and Table S1†). The adhesion energy was showing in case of the amino functionalised silica, SiO_2/–NH_2, two peaks at rather low values of about 0.06 fJ (typical of pure SiO_2 surface) and a slightly higher value 0.14 fJ, corresponding to the hydrophobic silicon nitride cantilever interaction with amino groups.

For the thiol functionalised sample, SiO_2/–SH, featured two major types of interaction with average energies 0.44 and 0.64 fJ. The mixed-ligand surface revealed more complex interaction, where two major contributions were at 0.27 fJ and 0.65 fJ. The latter is the same as in the thiol finished material, indicating the

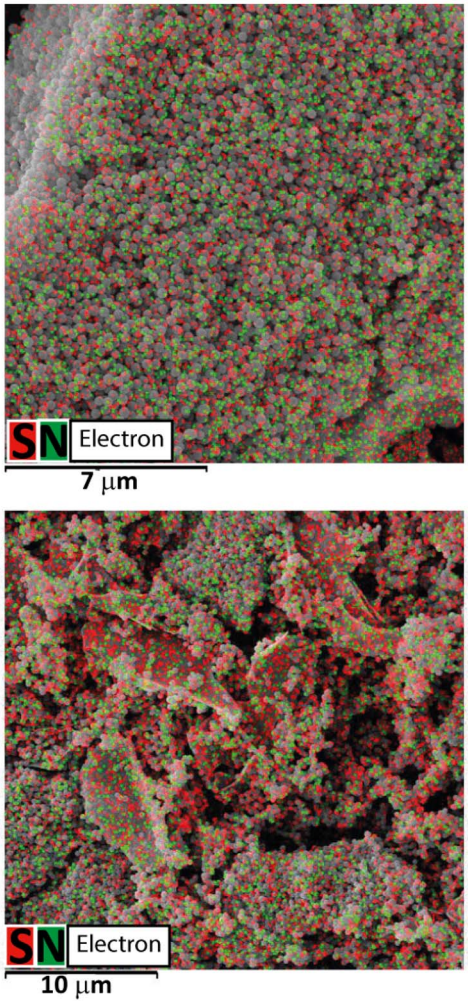

Fig. 4 Mapping of sulphur and nitrogen in the received suprastructure consisting of SiO_2/–SH/–NH_2 particles in 16 and 30 μm viewfields.

same surface characteristics of the thiol patches. The lower energy is higher than for amino group terminated surface, but still close to the original one, indicating that amino group terminated area is confined and less polar than in only amino group finished material. This effect would be the most probable reason for enhanced interaction energy with a hydrophobic cantilever.

To verify the adsorption properties of the attached groups, the adsorption of cations and anions that were both related to these groups and of interest for potential applications was investigated. Specifically, europium(III) ions[30] and fluorescein[31] were employed to bind with the amino groups, while silver(I)[32] and gold(III)[33] ions were utilised for the mercapto groups. In sequential adsorption, a sorbate was initially employed for the amino groups due to their sorption capacity at pH = 6. Subsequently, sorption was performed for the mercapto groups using Ag(I) or Au(III) ions in an acidic medium to prevent the protonation of the amino groups. The advantages of these particles lie in the sequential adsorption process: the interaction of Eu(III) or fluorescein primarily happens with amino groups followed by Ag(I) or Au(III) with mercapto groups. Consequently, a variety of compounds simultaneously exist on the surface, contributing to its multifunctionality.

Adsorption isotherms of the studied adsorbates on Janus silica particles are presented in Fig. 8. It was determined that the SiO_2/–SH/–NH_2 sample exhibits adsorption capacities of 61 mg g^{-1} (0.4 mmol g^{-1}) for Eu(III) ions and 58.3 mg g^{-1} (0.18 mmol g^{-1}) for fluorescein. Furthermore, the adsorption capacities were measured as 80.0 mg g^{-1} (0.41 mmol g^{-1}) for Au(III) and 48.4 mg g^{-1} (0.45 mmol g^{-1}) for Ag(I). Importantly, the presence of fluorescein or europium on the sample did not impact the sorption capacity for the adsorption of Au(III) or Ag(I) ions.

A confirmation of the adsorption by the sample is depicted in Fig. 9. Although the exact adsorption centres were challenging to identify, the presence of an equal number of groups and metals indicated that Eu(III) was taken up due to the amino groups, while Ag(I) and Au(III) were sorbed by the mercapto groups.

The changes that occurred with the groups and their involvement in various interactions were investigated using X-ray photoelectron spectroscopy, as presented in Table 2 and Fig. 10. The data obtained from XPS analysis have confirmed the presence of sulphur on the bifunctional silica surface in the

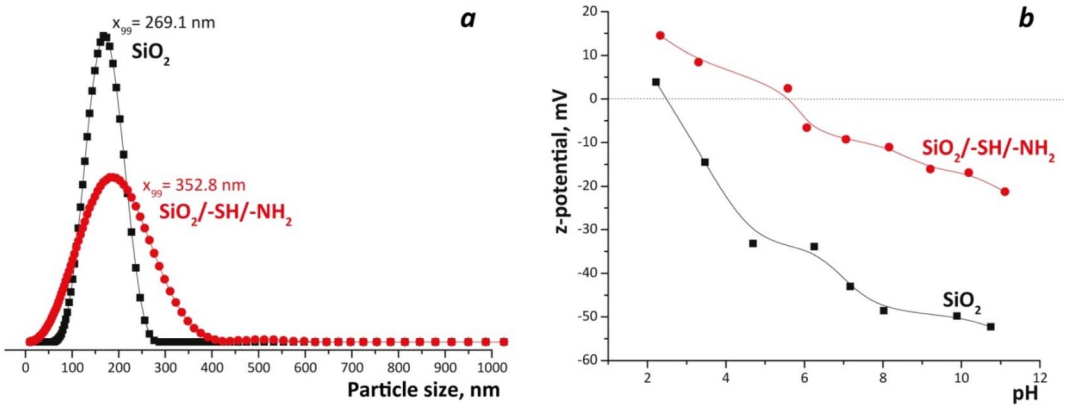

Fig. 5 Particle size distribution for SiO_2 and SiO_2/–SH/–NH_2 particles from PCCS data (a) and zeta-potential measurements (b).

Table 1 Content of groups in the synthesised sample

Sample	SiO_2/APTMS/MPTMS ratio	Synthetic ratio, mmol g^{-1}		Elemental analysis, mmol g^{-1}		DTNBA and H^+ interaction, mmol g^{-1}		EDXS, mmol g^{-1}		XPS, mmol g^{-1}	
		C_{SH}	C_{NH_2}	C_{SH}	C_{NH_2}	C_{SH}	C_{NH_2}	C_{SH}	C_{NH_2}	C_{SH}	C_{NH_2}
SiO_2/–SH/–NH_2	2.8/1/1	2.75	2.75	2.0	2.0	1.7	2.2	0.6	1.9	1.9	2.2

form of thiol –SH with S 2p binding energy (BE) 163.6 eV and –NH_2 surface groups in protonated (401.6 eV) and non-protonated (399.5 eV) forms (Table 2).

The availability of non-hydrolysed silane precursors was observed in the O 1s spectrum with a BE of 532.7 eV, which coincided with the IR observations. The XPS spectra of the samples after adsorption of fluorescein, Ag^+, Au^{3+}, and Eu^{3+} ions displayed notable shifts in the binding energies of the functional groups. Thus, the shift in BE of protonated amino groups after fluorescein adsorption demonstrated their predominant effect in fluorescein's elimination. No other shifts could be observed, which proved this statement. According to XPS analysis, silver was bonded to active thiol adsorption centres and formed argentum(I) sulphide[34] with a small shift in the BE of amino groups caused by their protonation since the initial solution of $AgNO_3$ was prepared in an acidic medium. The presence of nitrate ions on the XPS spectrum was explained by the use of silver nitrate in adsorption experiments. It was of interest to note that the formation of oxidised sulphur species had been identified on several samples (see Fig. 10).

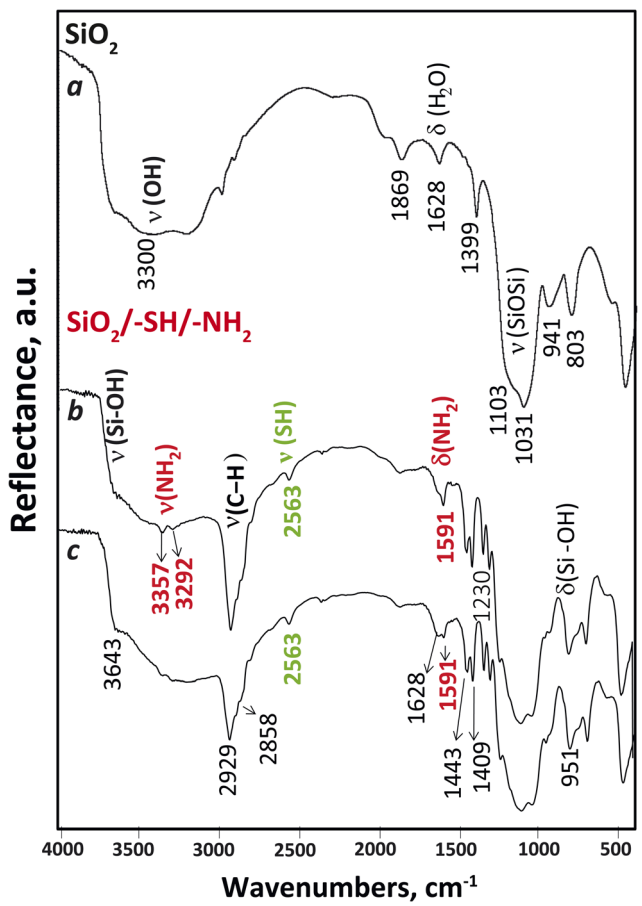

Fig. 6 FTIR spectra of SiO_2 nanoparticles (a) at 100 °C and SiO_2 nanoparticles functionalised with amino and mercapto groups at 100 °C (b) and 25 °C (c).

Indeed, a split in the S 2p BE to 168.1 eV and 163.2 eV was recorded on the spectrum of the sample loaded with Ag^+. The peak with lower energy was related to the thiol moieties of the material, and the noticed shift (Δ = 0.4 eV) evidenced the formation of chemical bonds between silver and –SH groups. The changes in the BEs of C–N/C–S bonds from 286.3 eV to 287.0 eV also verified the interaction of silver ions and thiol surface groups. The unexpected peak with higher energy at 168.1 eV that could be attributed to –SO_x species[35] was detected with a value of 2.2 at% (Tables S1–S7†). The same tendency was discovered for the samples with Au^{3+} and in the binary system Eu^{3+}/Ag^+ obtained by sequential adsorption (2.5 and 3.3 at%, respectively).

The formation of oxygen-containing sulphur species on the materials' surface could also be testified by increasing the atomic concentration of surface oxygen (Tables S2–S8†). The presence of single-ion Eu^{3+} did not show any oxidising effect on –SH surface groups since this metal possessed a high affinity towards amino groups,[30] which was established by a red shift of Δ = 0.3 eV in their BE. Therefore, under created conditions and in the presence of Ag^+ or Au^{3+}, the surface sulphur could be oxidised and form oxygen-containing species;[36] however, this issue requires further detailed studies. Additionally, the presence of oxygen-containing sulphur groups could improve the adsorption properties of the material towards rare earth metals.[37]

Desorption was conducted using complexing agents based on the formation of a complex with a higher stability constant. Specifically, for Au(III) and Ag(I) ions, acidified thiourea solutions were used. However, under these conditions, desorption reached 52% for Au(III) ions and 43% for Ag(I) ions, while the re-adsorption on the free sites was reduced to 48% of the possible free sites (*i.e.*, 20 mg g^{-1}) for gold ions and to 28% (*i.e.*, up to 3 mg g^{-1}) for silver ions. It appears that some groups form insoluble sulfides with Au(III) and Ag(I), or the ions are even rapidly reduced to nanoparticles in such environment.

Regarding the desorption of Eu(III) ions, it reached 76%, while the re-adsorption achieved 72% of the possible, amounting to 49 mg g^{-1}. The desorption of Fluorescein was 83% and reached 94% during the initial desorption with

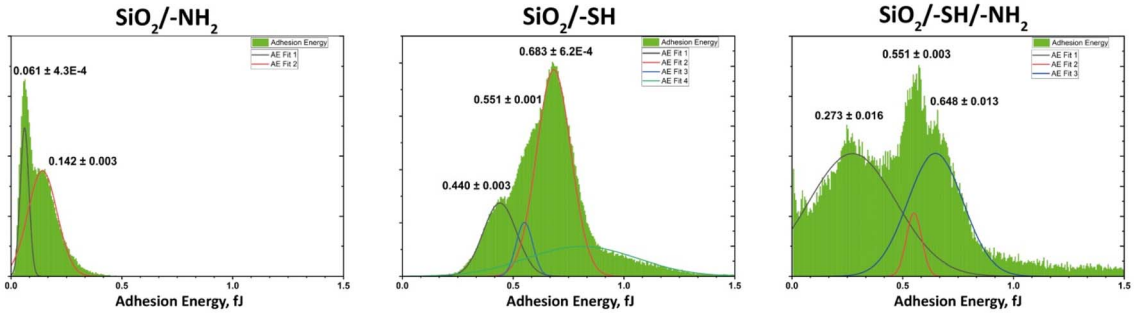

Fig. 7 Adhesion energy distribution on the surface of the samples (according to quantitative peak force measurement in AFM).

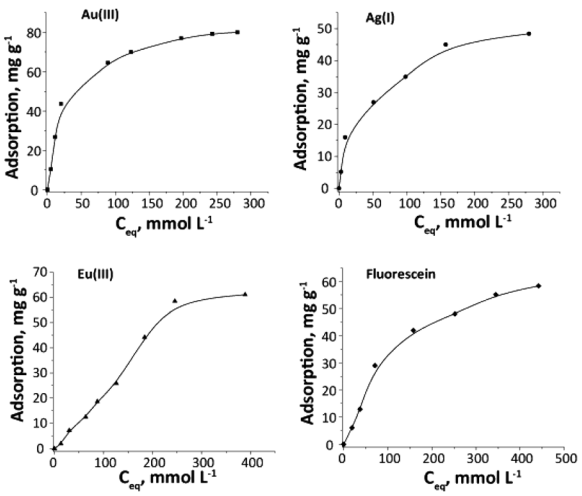

Fig. 8 Au(III), Ag(I), Eu(III) ions and fluorescein adsorption isotherms for SiO_2/–SH/–NH_2 particles.

thiourea in an acidic environment. This confirms the physical character of adsorption of the dye molecules on the surfaces the particles. The re-adsorption was 90%, amounting to 44 and 49 mg g^{-1}, respectively.

Therefore, while desorption may not be exceptionally effective for such systems, they appear to be promising for application as it is, with adsorbed cations and organic dyes.

To explore additional potential applications of the synthesised particles, we analysed the photoluminescence spectra of aqueous suspensions of silica particles, as shown in Fig. 11. The ionic strength and sample concentration parameters were adopted from our previous studies.[43] As observed in Fig. 11a, the sample with adsorbed Eu(III) exhibits no characteristic peaks, similar to the antibiotic oxytetracycline at an excitation of 400 nm. However, the suspension containing the antibiotic demonstrates an increase in PL intensity, displaying characteristic peaks indicative of $^5D_0$–$^7F_{1-4}$ transitions in europium at 592, 616, 646, and 694 nm, respectively. Probes for the determination of tetracyclines are documented in the literature,[44] utilizing Eu(III) on the surface as antenna elements. However, these studies typically did not investigate selectivity in depth. As observed, the presence of Ag(I) ions or the blocking of sulphur-containing groups diminishes the 'antenna' properties. In the presence of Au(III) ions, only a single transition peak for Eu(III) is noted. These preliminary findings necessitate further examination of the impact of various factors on the photoluminescent properties of such suspensions. Interestingly, in the absence of oxytetracycline, the SiO_2/–SH/–NH_2 original silica particles with adsorbed Eu(III), Ag(I), and Au(III) ions exhibit no photoluminescent properties, as demonstrated in Fig. S3a.†

Unlike SiO_2/–SH/–NH_2 particles embedded with Eu(III), those doped with fluorescein exhibit PL even at half the sample concentration (Fig. 11b). Moreover, in the presence of the antibiotic norfloxacin (NR), PL intensity increases, making them potential candidates for detecting this substance in solutions. At an excitation wavelength of 400 nm, particles additionally loaded with Ag(I) and Au(III) ions fail to function as sensors for NR. However, at an excitation of 480 nm (Fig. S3b†) at NR presence, PL significantly increases, indicating that, in samples doped with both Au(III) and fluorescein and Ag(I) alongside fluorescein, the PL can serve as a quantitative sensor for a drug concentration.

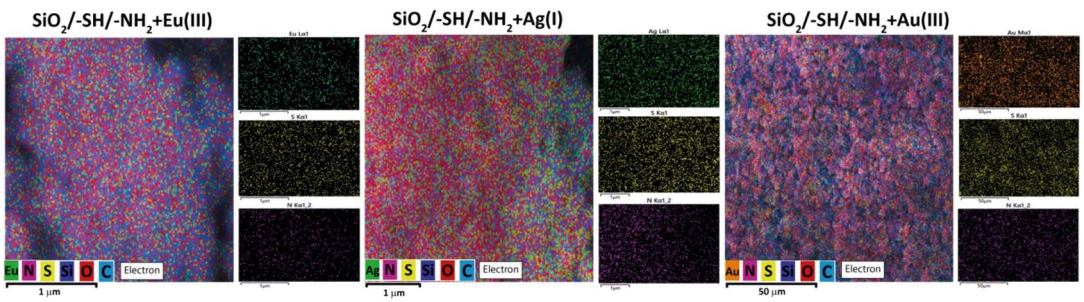

Fig. 9 EDXS element maps for ions loaded SiO_2/–SH/–NH_2 sample (Eu^{3+}, Ag^+, Au^{3+}).

Table 2 Summary of XPS analysis of bare and loaded samples

	Binding energy, eV and assignment					
Sample	S 2p	C 1s	N 1s	O 1s	Si 2p	Element
SiO_2/–SH/–NH_2	163.6 thiol –SH	286.3 C–N/C–S 285.0 C–C	401.6 –NH_3^+ 399.5 C–NH_2	532.7 Si–O–C	103.2 Si^{4+}	—
+Fluorescein	163.6 thiol –SH	286.1 C–N/C–S 285.0 C–C	401.9 –NH_3^+ 399.5 C–NH_2	532.9 Si–O–C 531.0 Si–OH	103.4 Si^{4+}	—
+Ag^+	168.1 –SO_x 163.2 thiol –SH	287.0 C–N/C–S 285.0 C–C	407.3 NO_3^- 401.9 –NH_3^+ 399.7 C–NH_2	532.7 Si–O–C 531.4 Si–OH	103.3 Si^{4+}	Ag^+ 368.6
+Fluorescein/Ag^+	168.1 –SO_x 163.1 thiol –SH	288.6 C–S–O 286.8 C–N/C–S 285.0 C–C	409.1 NO_3^- 401.9 –NH_3^+ 400.0 C–NH_2	532.8 Si–O–C 531.7 Si–OH	103.3 Si^{4+}	Ag^+ 368.6
+Au^{3+}	168.0 –SO_x 163.4 thiol –SH	289.0 C–S–O 286.6 C–N/C–S 285.0 C–C	401.9 –NH_3^+ 400.0 C–NH_2	532.7 Si–O–C 531.2 Si–OH	103.3 Si^{4+}	Au^{3+} 85.0
+Eu^{3+}	163.7 thiol –SH	286.8 C–N/C–S 285.0 C–C	407.1 NO_3^- 400.9 –NH_3^+ 399.2 C–NH_2	532.8 Si–O–C 531.7 Si–OH	103.3 Si^{4+}	Eu^{3+} 1135.6
+Eu^{3+}/+Au^{3+}	168.3 –SO_x 163.2 thiol –SH	286.5 C–N/C–S 285.0 C–C	402.3 –NH_3^+ 400.5 C–NH_2	532.9 Si–O–C 531.7 Si–OH	103.4 Si^{4+}	Eu^{3+} 1135.6 Au^{3+} 85.0

Furthermore, particles solely loaded with silver(I) or gold(III) ions, when excited at 480 nm, display pronounced peaks at 515 nm and 522 nm, respectively (Fig. S3c†). Yet, an excitation of 400 nm is preferred for particles containing only silver, as the intensity values are more conducive to quantitative analysis (Fig. S3d†).

Therefore, various combinations of adsorbed ions and dyes unveil new potentials for Janus particles, warranting further detailed investigation.

To sum up, the obtained material possessed patchy surface with a combination of characteristics of hard and soft ligands. It demonstrates significant potential in the removal of organic and inorganic species owing to its dual switchable nature that expanded its adsorption properties. Concurrently, this approach holds potential for use in detecting pharmaceuticals in aqueous solutions as a sensor.

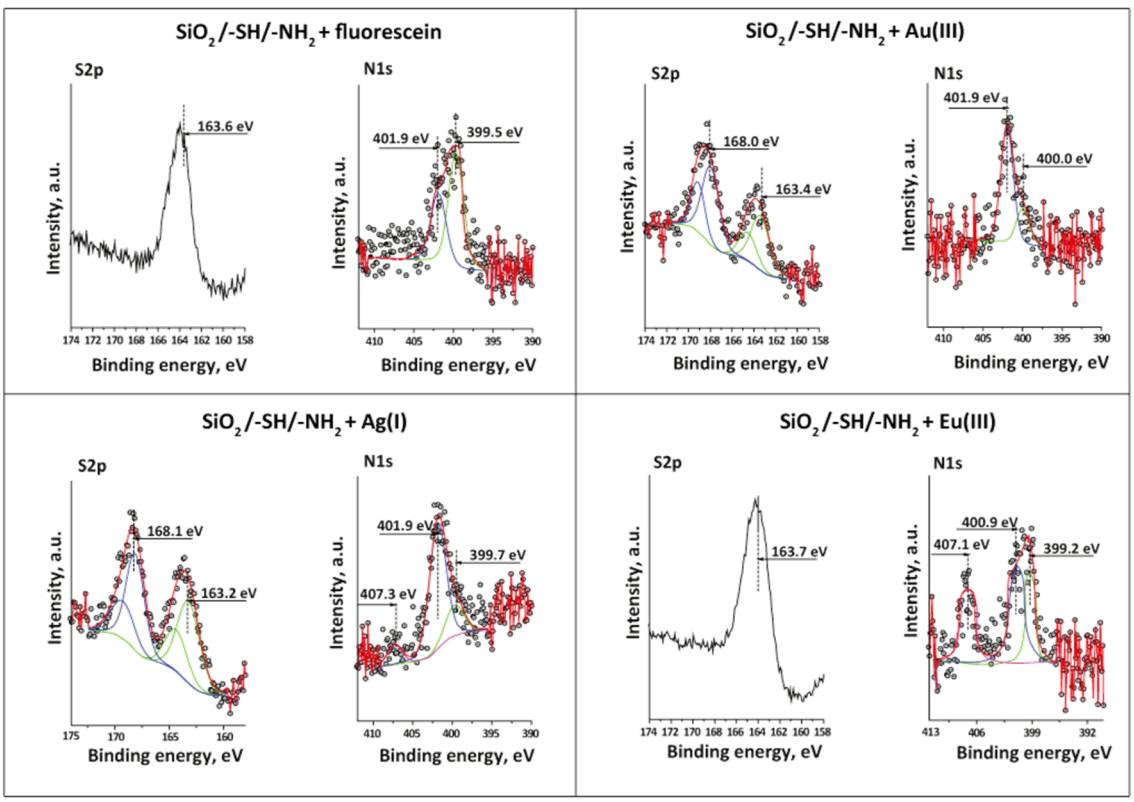

Fig. 10 S 2p and N 1s XPS spectra of SiO_2/–SH/–NH_2 samples loaded with cations and fluorescein.

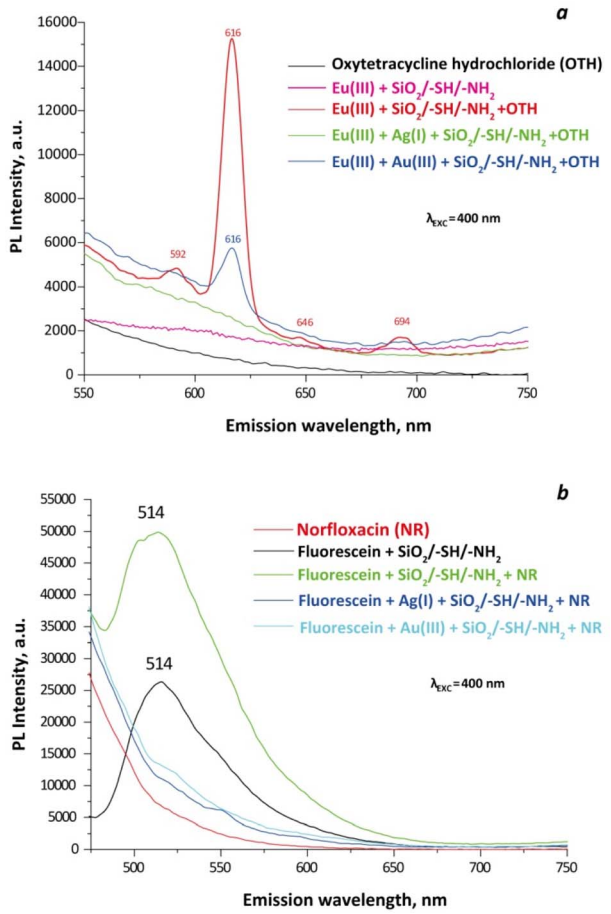

Fig. 11 Photoluminescence spectra of aqueous solutions of antibiotics and aqueous suspensions of Janus particles with adsorbed Eu(III) (a) (C_{sample} = 0.1 g L^{-1}) and fluorescein (b) (C_{sample} = 0.05 g L^{-1}) at an ionic strength of 0.1 M.

Experimental

Sample preparation

Reagents for synthesis: tetraethyl orthosilicate, $Si(OC_2H_5)_4$ (TEOS, 99%, Aldrich); (3-mercaptopropyl)trimethoxysilane, $HS(CH_2)_3Si(OCH_3)_3$ (MPTMS, 95%, Aldrich); (3-aminopropyl) trimethoxysilane, $H_2N(CH_2)_3Si(OCH_3)_3$ (APTMS, 97%, Aldrich); ammonium hydroxide solution, NH_4OH (25% analytical reagent grade, Fisher Chemical); sodium fluoride, NaF (99%, ITES); hydrochloric acid, HCl (35%, Aldrich); sodium hydroxide, NaOH (p.a., microCHEM); ethyl alcohol, C_2H_5OH (96%, microCHEM); and toluene, $C_6H_5CH_3$ (99.5%, Alfa Aesar).

Reagents that were used in the sorption process and PL: silver(I) nitrate, $AgNO_3$ (pure p.a., microCHEM); nitric acid, HNO_3 (65%, for analysis, microCHEM); hydrogen tetrachloroaurate hydrate, $H[AuCl_4]\cdot H_2O$ (99.999%, trace metals basis, Acros Organics); fluorescein, $C_{20}H_{12}O_5$ (95%, Aldrich); europium(III) nitrate hexahydrate, $Eu(NO_3)_3\cdot 6H_2O$ (99.9%, Alfa Aesar); 5,5′-dithiobis-(2-nitrobenzoic acid), $C_{14}H_8N_2O_8S_2$ (DTNBA, 99%, Acros organics); methanol, CH_3OH (p.a., microCHEM); trimethylamine, $C_6H_{15}N$ (99%, Aldrich); methyl orange, $C_{14}H_{14}N_3NaO_3S$ (p.a., microCHEM); potassium chloride, KCl (99.5%, mikroCHEM); norfloxacin $C_{16}H_{18}FN_3O_3$ (98%, ThermoScientific); oxytetracycline hydrochloride $C_{22}H_{25}ClN_2O_9$ (96%, ThermoScientific); thiourea CH_4N_2S (99%, p.a., Chemapol); chelation III $C_{10}H_{14}N_2Na_2O_8\cdot 2H_2O$ (99–100.5%, p.a., CelntralChem). All reagents were used as received without further purification.

Silica particles preparation and functionalisation conditions

A solution of 34.2 mL of H_2O and 28.67 mL of aqueous ammonia (25%) was prepared in 200 mL of ethanol and heated at 65 °C under N_2(g) atm. TEOS (11.16 mL) was then added with vigorous stirring. The reaction was continued for 1 h to obtain silica particles. The particles were separated by centrifugation at 10 000 rpm for 10 min then washed two times with water (40 mL) and one time with ethanol (40 mL). Afterward, the sample was dried under N_2(g) at room temperature overnight, and then at 100 °C in an oven for 24 h.

For silica particle functionalisation, 6 mL of toluene were mixed with 80 mL of milliQ water to prepare a toluene-in-water emulsion. Then, a batch of SiO_2 particles (0.1020 $g = 1.7$ mmol) was sonicated in 1 mL of toluene and was added to the emulsion. After stirring for 120 min, MPTMS (132 μL of MPTMS (0.6 mmol) + 132 μL of toluene + 132 μL of 0.0025 M HCl) and APTMS (114 μL of APTMS (0.6 mmol) + 114 μL of 0.1% NaF) were added together. After adding all reagents, the stirring was continued for 2 min and then stopped. The sample was separated by centrifugation after 18 h, washed with alcohol, and dried in a vacuum oven at 65 °C for 6 h.

Characterization

The imaging and the estimation of the amounts of ligand were carried out by the SEM-EDXS technique using a Hitachi TM-1000-μ-DeX tabletop and FlexSEM 1000 II scanning electron microscopes. The mapping of nitrogen (N) and sulfur (S) elements on the surface was also conducted using a Tescan Mira 3 LMU scanning electron microscope, equipped with an Energy-Dispersive X-ray (EDXS) Oxford X-max 80 mm detector. For the analysis, samples were mounted on a metal stub with an adhesive carbon tape and coated with 0.03 μm layer of gold using a Gatan Model 682 Precision Etching Coating System.

Surface structure of the modified sample was studied using a Bruker Dimension FastScan Bio Atomic Force Microscope (AFM) in ScanAsyst mode. Quantitative Peak Force Management (QPFM) – measurements were carried out with pre-calibrated silicon nitride cantilevers in adhesion mode. The force curves were analysed in the Digital Surf MountainsLab Premium 10 program. Data was processed using Origin Pro 2020, fitting a Gaussian model.

Granulometric analysis was carried out by photon cross-correlation spectroscopy (PCCS) using a Nanophox particle size analyser (Sympatec, Germany). A portion of the aqueous suspension of each sample was diluted with the stabiliser to achieve a suitable concentration for measurement. The measurements were repeated three times for each sample. Zeta potential measurements were conducted with a Zetasizer Nano ZS (Malvern, Great Britain).

The CHNS analysis was done using Vario MACRO cube elementary analyser (Elementar Analysensysteme GmbH, Germany) with a thermal conductivity detector.

FTIR spectra of powdery samples were recorded on a Thermo Nicolet Nexus FTIR spectrometer in the 400–4000 cm^{-1} range of wavenumbers and with a resolution of 8 cm^{-1}. The samples were ground with potassium bromide at a mass ratio of sample/KBr = 1/30.

Thermogravimetric analysis was carried out in air with a heating rate of 10 °C min^{-1} using a PerkinElmer Pyris-1 instrument.

Low-temperature nitrogen adsorption–desorption isotherms were recorded with a Quantachrome NOVA 1200e surface area and pore size analyser (USA). Before the measurements, the samples were degassed at 80 °C for 48 h in a vacuum. The BET-specific surface area was evaluated in the 0.05–0.35 range of relative pressures.

XPS measurements were carried out on an ESCALAB MkII (VG Scientific, now Thermo Scientific) electron spectrometer with a base pressure in the analysis chamber of 5×10^{-10} mbar (9×10^{-8} mbar during the measurements), equipped with twin anode Mg Kα/Al Kα non-monochromated X-ray source using excitation energies of 1253.6 and 1486.6 eV, respectively. The measurements are provided only with an Al Kα non-monochromated X-ray source (1486.6 eV). The pass energy of the hemispherical analyser was 20 eV; in cases of lower signal a 50 eV pass energy was used. The instrumental resolution measured as the full width at half maximum (FWHM) of the Ag $3d_{5/2}$ photoelectron peak is about 1 eV. The energy scale has been calibrated by normalising the C 1s line of hydrocarbons to 285.0 eV for electrostatic sample charging. The data was analysed by SpecsLab2 CasaXPS software (Casa Software Ltd). The processing of the measured spectra includes a subtraction of X-ray satellites and Shirley-type background.[38] The peak positions and areas are evaluated by a symmetrical Gaussian–Lorentzian curve fitting. The relative concentrations of the different chemical species are determined based on normalisation of the peak areas to their photoionisation cross-sections, calculated by Scofield.[39]

To determine the content of –SH groups, Ellman's reagent (5,5′-dithiobis-(2-nitrobenzoic acid)) was used:[40] 50 mg of the sample were added to 10 mL of methanol to obtain sample suspension. In parallel, 100 mg of Ellman's reagent were dissolved in 15 mL of methanol and then 0.25 mL of triethylamine were added. Next, the sample suspension and Ellman's reagent solution were mixed and stirred for 30 min. An analysed mixture was filtered through a Whatman filter before the measurements. The 2-nitro-5-thiobenzoate anion absorbance was measured at 412 nm on a Helios Gamma UV-vis spectrophotometer (l = 1 cm) (Thermo electron corporation, UK). The amount of available –SH surface groups was calculated from Beer's law, $A = \varepsilon \cdot l \cdot C$, assuming that the extinction coefficient of the 2-nitro-5-thiobenzoate anion is equal to ε = 14 150 M^{-1} cm^{-1}.[41] The accuracy of the method was controlled by the same reaction of Ellman's reagent with a definite amount of (3-mercaptopropyl)trimethoxysilane in methanol.

To determine the content of $-NH_2$ groups, the method of acid–base back titration was applied.[42] It is based on the determination of the number of protons absorbed by the amino groups after holding the sorbent batch (0.05 g) in an excess of 0.05 M HCl solution for 24 h. The excess hydrochloric acid was titrated with 0.05 M NaOH with methyl orange as an indicator.

The study on the adsorption of fluorescein was carried out with 0.01 g of SiO_2/–SH/$-NH_2$ silica particles added to 10.0 mL (0.075–1.5 mM solution) of dye at pH ~6 in a static mode. The sample was collected in 24 h, and the fluorescein absorbance was measured at 481 nm on a Helios Gamma UV-vis spectrophotometer (Thermo electron corporation, UK).

The functionalised particles that were produced were tested for the adsorption of metal ions (Ag^+, Au^{3+}, Eu^{3+}) from water solutions. The mass of the sample, the volume of the solution, and the concentrations were the same for 0.01 g, 10 mL, and 0.1–1.5 mM of fluorescein, respectively. Only, for solutions of Ag^+ and Au^{3+}, pH was 3. The content of Ag^+ and Au^{3+} ions in the solution before and after sorption was determined by the atomic absorption spectrometer Varian AA 240 FS. The amount of adsorbed Europium(III) was quantified by Agilent Technologies 7700 Series ICP-MS.

Desorption studies were performed using different desorbing agents, depending on the nature of the substance to be desorbed. Thus, for the elution of Au(III) ions, the samples were dynamically stirred with a 1% thiourea solution in 0.01 M HCl. Desorption of Ag(I) ions was carried with a 1% thiourea solution in 0.01 M HNO_3. The Eu(III) ions were removed with a 0.01 M solution of chelation III, while an acidified methanol solution was employed for fluorescein. The concentrations of desorbates were determined as described earlier in the adsorption paragraph. In order to analyse the desorption of two types of substances present on the surface, the procedure was conducted in two stages: initially desorbing the Au(III) or Ag(I) ions, followed by Eu(III) or fluorescein.

Room temperature photoluminescence (PL) spectra were acquired on a photon-counting spectrofluorometer PC1 (ISS, USA) with a photoexcitation wavelength of 400 or 480 nm (resolution step 2 nm). A 300 W xenon lamp was used as the excitation source. Excitation and emission slit widths were set at 1.0 and 1.0 mm. The samples were placed into 1 cm path length rectangular quartz cuvette for spectral analysis. Aqueous suspensions used for measuring PL spectra were prepared at an ionic strength of 0.1 M, achieved through the addition of KCl. The concentration of the suspensions was set to either 0.05 g L^{-1} or 0.1 g L^{-1} of the sample. In experiments involving antibiotics, their concentration was maintained at 6 mg L^{-1}, with the ionic strength kept constant at 0.1 M.

Conclusions

Silica particles with a designed structure, functionalised with amino and mercapto surface groups, were successfully synthesised using a two-step procedure. The characterisation of these particles was performed using various advanced analytical techniques. Analysis of SEM and AFM data revealed that the final particles consisted of three hierarchical levels: primary

small spherical particles (5–10 nm) that formed secondary globules with a size of 350 nm, which in turn assembled into tertiary suprastructures measuring approximately 30 μm. SEM-EDXS mapping provided valuable insights into the distribution of sulphur and nitrogen on the material's surface, indicating a patch-like arrangement. Consequently, the material could be identified as Janus patches. The content of amino and mercapto groups was quantified through elemental analysis, EDXS, XPS, titration, and spectrophotometric data. The results indicated an approximate amount of 2 mmol g^{-1} for each group. The presence of –SH and $–NH_2$ groups in the surface layer of the sample was confirmed through IR spectra. Additionally, sorption and desorption studies involving Eu(III), Au(III), and Ag(I) demonstrated varying interactions between these groups and different metal ions. XPS analysis further validated the obtained results, revealing an intriguing observation regarding the oxidation of surface thiol groups in the presence of Ag(I) and Au(III). This research highlights the sustainable nature of Janus particles and their significant potential in environmentally friendly applications, which have not yet been fully explored.

Author contributions

All authors conceived and designed the research. Inna V. Melnyk: conceptualisation, formal analysis, resources, writing – original draft, supervision; Veronika Tomina: methodology, formal analysis, investigation, writing – original draft; Halyna Yankovych: formal analysis, investigation, writing – original draft; Hristo Kolev: formal analysis, investigation; Erika Dutkova: formal analysis, investigation; Troy C. Breijaert: formal analysis, investigation; Vadim G. Kessler: resources, writing – review & editing, project administration; Gulaim A. Seisenbaeva: conceptualisation, formal analysis, investigation, resources, writing – review & editing, supervision. All authors read and approved the manuscript.

Conflicts of interest

There are no conflicts to declare.

Acknowledgements

The authors express their gratitude to the Swedish Research Council grant DNr. 2018-04841 (Sweden) and APVV-19-0302 project (Slovakia) for the support of the current research.

References

1 A. Walther and A. H. E. Müller, *Chem. Rev.*, 2013, **113**, 5194.
2 J. Hu, S. Zhou, Y. Sun, X. Fang and L. Wu, *Chem. Soc. Rev.*, 2012, **41**, 4356.
3 S. Jiang, Q. Chen, M. Tripathy, E. Luijten, K. S. Schweizer and S. Granick, *Adv. Mater.*, 2010, **22**, 1060.
4 B. P. Binks and S. O. Lumsdon, *Langmuir*, 2000, **16**, 2539.
5 L. Liu, W. Yao, X. Xie, J. Gao and X. Lu, *J. Nanobiotechnol.*, 2021, **19**, 235.
6 Q. He, H. Vijayamohanan, J. Li and T. M. Swager, *J. Am. Chem. Soc.*, 2022, **144**, 5661.
7 M. Gigliotti, G. Schmidt-Traub and S. Bastianoni, in *Encyclopedia of Ecology*, ed. B. Fath, Oxford, Elsevier, 2nd edn, 2019, 426–431.
8 C. Marschelke, A. Fery and A. Synytska, *Colloid Polym. Sci.*, 2020, **298**, 841.
9 W. Gao and J. Wang, *ACS Nano*, 2014, **8**, 3170.
10 L. Zhao, S. Xie, Y. Liu, Q. Liu, X. Song and X. Li, *Nanoscale*, 2019, **11**, 17831.
11 F. Zheng, W. Ke, L. Shi, H. Liu and Y. Zhao, *Anal. Chem.*, 2019, **91**, 11812.
12 D. H. Kang, H. S. Jung, N. Ahn, S. M. Yang, S. Seo, K. Y. Suh, P. S. Chang, N. L. Jeon, J. Kim and K. Kim, *ACS Appl. Mater. Interfaces*, 2014, **63**, 10631.
13 L. Wang, A. Kaeppler, D. Fischer and J. Simmchen, *ACS Appl. Mater. Interfaces*, 2019, **11**, 32937.
14 Q. Yuan, D. Liu, N. Zhang, W. Ye, H. Ju, L. Shi, R. Long, J. Zhu and Y. Xiong, *Angew. Chem., Int. Ed. Engl.*, 2017, **56**, 4206.
15 P. Yánez-Sedeño, S. Campuzano and J. M. Pingarrón, *Appl. Mater. Today*, 2017, **9**, 276.
16 Y. L. Zub, I. V. Melnyk, M. G. White and B. Alonso, *Adsorpt. Sci. Technol.*, 2008, **26**, 119.
17 N. V. Stolyarchuk, I. V. Mel'nik, Y. L. Zub, M. Barczak, A. Dabrowski and B. Alonso, *Prot. Met. Phys. Chem. Surf.*, 2009, **45**, 169.
18 I. V. Melnyk, N. V. Stolyarchuk, V. V. Tomina, O. Bespalko and M. Vaclavikova, *Appl. Nanosci.*, 2020, **10**, 2813.
19 N. Tang, X. Liu, M.-R. Jia, X.-Y. Shi, J.-W. Fu, D.-X. Guan and L. Q. Ma, *Chemosphere*, 2022, **291**, 132771.
20 S.-J. Chiu, S.-Y. Wang, H.-C. Chou, Y. G.-L. Liu and T.-M. Hu, *Langmuir*, 2014, **30**, 7676.
21 E. Boyacı, A. Çağır, T. Shahwan and A. E. Eroğlu, *Talanta*, 2011, **85**, 1517.
22 K. Y. Shi, W. M. Hou and H. Y. Zhao, *Polymer*, 2022, **240**, 124487.
23 W. Stöber, A. Fink and E. Bohn, *J. Colloid Interface Sci.*, 1968, **26**, 62.
24 E. Piccinini, D. Pallarola, F. Battaglinic and O. Azzaron, *Mol. Syst. Des. Eng.*, 2016, **1**, 155.
25 C. Kang and A. Honciuc, *J. Phys. Chem. Lett.*, 2018, **9**, 1415.
26 J. S. Oh, S. Lee, S. C. Glotzer, G.-R. Yi and D. J. Pine, *Nat. Commun.*, 2019, **10**, 3936.
27 K. S. Sing, *Pure Appl. Chem.*, 1985, **57**, 603.
28 B. Baumgartner, J. Hayden, A. Schwaighofer and B. Lendl, *ACS Appl. Nano Mater.*, 2018, **1**, 7083.
29 **https://www.sigmaaldrich.com/SK/en/technical-documents/technical-article/analytical-chemistry/photometry-and-reflectometry/ir-spectrum-table**.
30 V. V. Tomina, N. V. Stolyarchuk, A. Katelnikovas, M. Misevicius, M. Kanuchova, A. Kareiva, A. Beganskienė and I. V. Melnyk, *Colloids Surf., A*, 2021, **608**, 125552.
31 I. V. Melnyk, V. V. Tomina, N. V. Stolyarchuk, G. A. Seisenbaeva and V. G. Kessler, *J. Mol. Liq.*, 2021, **336**, 116301.

32 N. V. Stolyarchuk, H. Kolev, M. Kanuchova, R. Keller, M. Vaclavikova and I. V. Melnyk, *Colloids Surf., A*, 2018, **538**, 694.
33 M. Kalantari, T. Ghosh, Y. Liu, J. Zhang, J. Zou, C. Lei and C. Yu, *ACS Appl. Mater. Interfaces*, 2019, **11**, 13264.
34 A. Arulraj, N. Ilayaraja, V. Rajeshkumar and M. Ramesh, *Sci. Rep.*, 2019, **9**, 10108.
35 S. Baik, H. Zhang, Y. K. Kim, D. Harbottle and J. W. Lee, *RSC Adv.*, 2017, **7**, 54546.
36 R. Qu, C. Sun, C. Ji, Q. Xu, C. Wang and G. Cheng, *Eur. Polym. J.*, 2006, **42**, 254.
37 I. Anastopoulos, A. Bhatnagar and E. C. Lima, *J. Mol. Liq.*, 2016, **221**, 954.
38 D. Shirley, *Phys. Rev. B: Solid State*, 1972, **5**, 4709.
39 J. H. Scofield, *J. Electron Spectrosc. Relat. Phenom.*, 1976, **8**, 129.
40 R. P. Hodgkins, A. E. Garcia-Bennett and P. A. Wright, *Microporous Mesoporous Mater.*, 2005, **79**, 241.
41 K. Güçlü, M. Özyürek, N. Güngör, S. Baki and R. Apak, *Anal. Chim. Acta*, 2013, **794**, 90.
42 J. J. Yang, I. M. El-Nahhal, I.-S. Chuang and G. E. Maciel, *J. Non-Cryst. Solids*, 1997, **209**, 19.
43 H. Yankovych, E. Dutková, V. Kyshkarova, M. Vaclavikova and I. Melnyk, *Chemosensors*, 2023, **11**, 332.
44 L.-H. Duan, J. Wang, Q. Zhao, J. Yang, Y. Zhou and H.-B. Liu, *Spectrochim. Acta, Part A*, 2024, **307**, 123638.